SF2A 2023
M. N'Diaye, A. Siebert, N. Lagarde, O. Venot, K. Baillié, M. Béthermin, E. Lagadec, J. Malzac, J. Richard (eds)

NEBULAR SPECTRA FROM TYPE Ia SUPERNOVA EXPLOSION MODELS COMPARED TO JWST OBSERVATIONS OF SN 2021aefx

S. Blondin[1], L. Dessart[2], D. J. Hillier[3], C. A. Ramsbottom[4] and P. J. Storey[5]

Abstract. Recent *JWST* observations of the Type Ia supernova (SN Ia) 2021aefx in the nebular phase have paved the way for late-time studies covering the full optical to mid-infrared (MIR) wavelength range, and with it the hope to better constrain SN Ia explosion mechanisms. We investigate whether public SN Ia models covering a broad range of progenitor scenarios and explosion mechanisms can reproduce the full optical-MIR spectrum of SN 2021aefx at $\sim$270 days post explosion. We performed 1D steady-state non-local thermodynamic equilibrium simulations with the radiative-transfer code CMFGEN, and compared the predicted spectra to SN 2021aefx. Taken as a whole, the models can explain the main features of this SN over the full wavelength range. However, no single model emerges as a preferred match. We discuss possible causes for the mismatch of the models, including ejecta asymmetries and ionisation effects. Our models suggest that key physical ingredients are missing from either the explosion models, or the radiative-transfer post-processing, or both. Nonetheless, they also show the potential of the near- and MIR to uncover new spectroscopic diagnostics of SN Ia explosion mechanisms.

Keywords: supernovae: general, Radiative transfer, Atomic data, Line: identification, supernovae: individual: SN 2021aefx

1 Introduction

Current models for Type Ia supernovae (SNe Ia) invoke variations in the mass of the exploding carbon-oxygen white dwarf (WD) and in the conditions of the thermonuclear runaway. These models include delayed detonations in near-Chandrasekhar-mass ($M_{\rm Ch}$) WDs double detonations in sub-$M_{\rm Ch}$ WDs, and violent mergers of two sub-$M_{\rm Ch}$ WDs. However, due to numerous degeneracies in SN Ia light curves and spectra, distinguishing between these various models has been a challenge (e.g. Maoz et al. 2014).

While the early high-brightness phase of SNe Ia ($\lesssim$ 50 d post explosion) yields constraints on the ejecta mass and kinetic energy, as well as the yields of intermediate-mass elements (IMEs) and ^{56}Ni, the late nebular phase ($>$ 100 d post explosion) can provide complementary information. At such times, the ejecta have expanded and diluted to become optically thin, revealing their innermost layers. The cooling is then dominated by forbidden lines that provide key nucleosynthetic information. In particular, the abundance of stable iron-group elements (IGEs) synthesised during the explosion has been proposed to distinguish sub-$M_{\rm Ch}$ from $M_{\rm Ch}$ progenitors, since their production increases with the central density (and hence initial mass) of the exploding WD (e.g. Flörs et al. 2020). Accurate abundance determinations are however difficult to obtain given the amount of line overlap and the sensitivity of line strengths to small variations in the ionisation state (Blondin et al. 2022). The advent of *JWST* has paved the way for systematic studies of SNe Ia in the mid-infrared (MIR), where lines are typically less blended (and less sensitive to the electron temperature) than in the optical and near-infrared

[1] Aix Marseille Univ, CNRS, CNES, LAM, Marseille, France
[2] Institut d'Astrophysique de Paris, CNRS-Sorbonne Université, 98 bis boulevard Arago, 75014, Paris, France
[3] Department of Physics and Astronomy & Pittsburgh Particle Physics, Astrophysics, and Cosmology Center (PITT PACC), University of Pittsburgh, 3941 O'Hara Street, Pittsburgh, PA 15260, USA
[4] Astrophysics Research Centre, School of Mathematics and Physics, Queen's University Belfast, Belfast BT7 1NN, Northern Ireland, UK
[5] Department of Physics and Astronomy, University College London, Gower Street, London WC1E 6BT, UK

© Société Française d'Astronomie et d'Astrophysique (SF2A) 2023

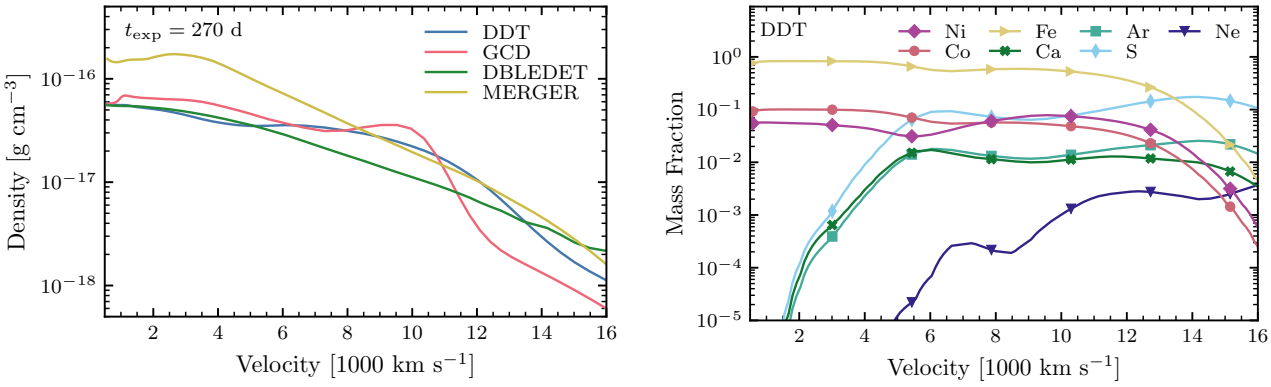

Fig. 1. Density profiles at 270 d post explosion for all models (*left*) and abundance profiles for the DDT model (*right*).

(NIR). This allows for a more secure identification of lines as well as detailed studies of their morphology, which may constrain the spatial distribution of the emitting material.

The Type Ia SN 2021aefx was recently observed with *JWST* using the Near Infrared Spectrograph (NIRSpec) and the Mid Infrared Instrument (MIRI) (Kwok et al. 2023a). Its nebular spectrum at +255 d past maximum light ($\sim$270 d post explosion) revealed the presence of numerous forbidden lines of IGEs and a distinct line due to argon ([Ar III] 8.99 μm), whose flat-topped profile was interpreted as indicative of a chemically stratified ejecta. Here we compare a diverse set of state-of-the-art, public SN Ia explosion models with the full optical-MIR nebular spectrum of SN 2021aefx, and evaluate which one, if any, fares better. All model outputs are publicly available online*, and the results presented here are taken from a recently accepted paper (Blondin et al. 2023).

2 Numerical approach

We select previously-published models from the Heidelberg Supernova Model Archive (HESMA; Kromer et al. 2017). These include the $M_{\rm Ch}$ delayed-detonation model N100 of Seitenzahl et al. (2013) [hereafter DDT], the $M_{\rm Ch}$ pulsationally assisted gravitationally-confined detonation model r10_d1.0 of Lach et al. (2022) [hereafter GCD], the sub-$M_{\rm Ch}$ double-detonation model M1002 of Gronow et al. (2021) [hereafter DBLEDET], and the violent merger model of Pakmor et al. (2012) [hereafter MERGER]. All models correspond to spherically-averaged versions of a 3D simulation. This averaging causes a systematic overestimate of the total mass by 3–8% and a difference of up to $\pm$10% for several isotopic and elemental yields compared to the original 3D models. The spherically-averaged density and representative abundance profiles at 270 d post explosion are shown in Fig. 1. We then solve the 1D non-local thermodynamic equilibrium (non-LTE) radiative transfer with CMFGEN (see Blondin et al. 2023, for details).

3 Results

Figure 2 shows the synthetic spectra for the four models compared to SN 2021aefx at 270 d post explosion in the wavelength range 0.35–14 μm. The models predict all the observed spectral features of SN 2021aefx from the blue end of the optical until the red end of the *JWST* range. Unfortunately, no single model produces a perfect match. The modest difference between the spectral properties of these four distinct explosion models reflects the similarity in composition for the dominant coolants in the ejecta. There are, however, numerous offsets in specific lines or features that result from differences in the abundance and ionisation of specific elements.

Throughout the optical and IR ranges, the spectrum is dominated by forbidden lines. Some exhibit clearly a broad flat top, e.g. [Ar III] 8.99 μm (except in the MERGER model), indicating a formation starting at large velocities and possibly extending to even larger velocities (the corresponding models have little Ar below about 5000 km s^{-1} or exhibit an ionisation stratification). Numerous lines show a Gaussian-like profile because they form throughout the ejecta (e.g. [Fe III] 0.47 μm). All lines from IGEs have typical line widths in the range $\sim$8000–14000 km s^{-1}, while those of IMEs, which tend to be present at large velocities only, exhibit significantly

*https://zenodo.org/record/8290155

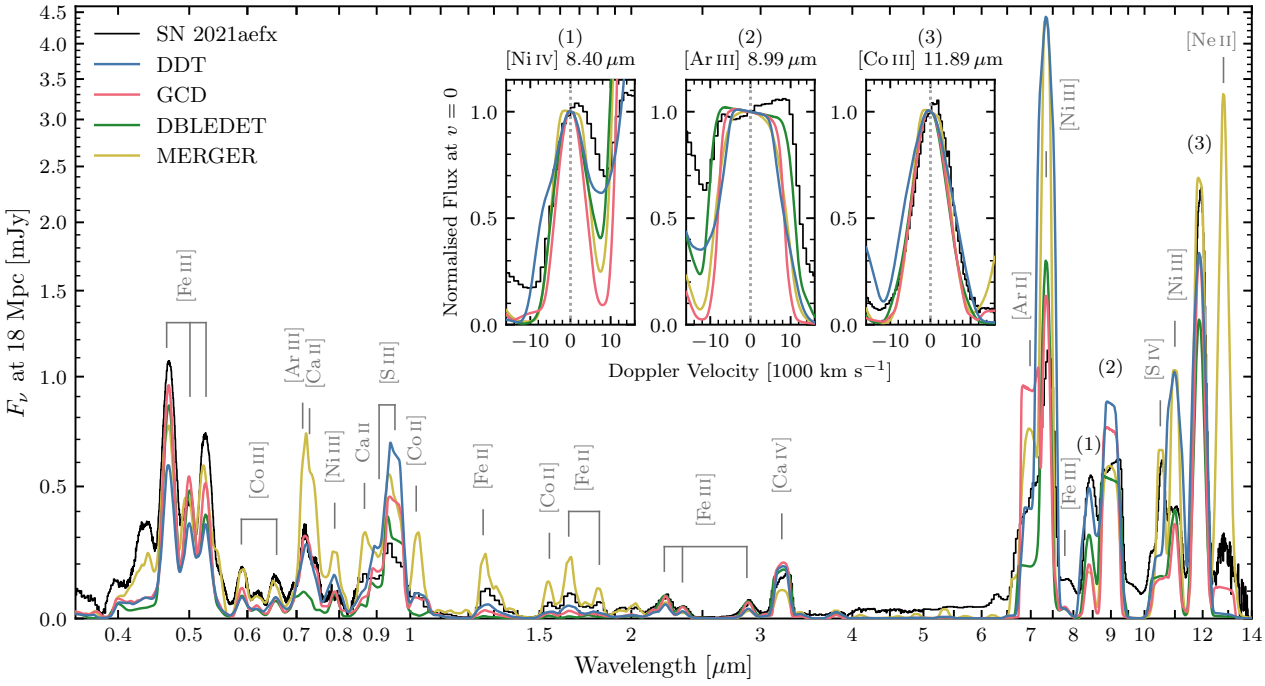

Fig. 2. Spectra of our four models at 270 days post explosion compared to SN 2021aefx over the wavelength range 0.35–14 μm. The SN 2021aefx spectrum has been corrected for redshift and extinction (assuming a host-galaxy reddening of 0.097 mag and a MW reddening of 0.008 mag). The synthetic fluxes correspond to the same assumed distance to SN 2021aefx of 18 Mpc; they have not been rescaled or normalised in any way. We include selected line identifications based on their maximum Sobolev equivalent width. The insets show normalised line profiles in velocity space for selected transitions, illustrating variations in line widths and morphology.

larger widths (FWHM $\gtrsim 20000\,\mathrm{km\,s^{-1}}$). The inset in Figure 2 gives the typical profile morphologies in our model spectra, using [Ni IV] 8.40 μm, [Ar III] 8.99 μm, and [Co III] 11.89 μm.

Our MERGER model displays a very strong line due to [Ne II] 12.81 μm, whose peaked profile reflects the presence of neon all the way to the innermost region of the ejecta. This is a natural expectation of this model as the central ejecta is dominated by the ashes of the secondary WD which burns to O and IMEs (Pakmor et al. 2012). While inconsistent with SN 2021aefx, this line was recently detected in the nebular spectrum of another SN Ia, which was interpreted as a violent merger event (SN 2022pul; Kwok et al. 2023b).

We attempted to qualitatively evaluate the impact of ejecta asymmetries on our 1D modelling approach by considering different directions in the original 3D version of the DDT model (I. Seitenzahl, priv. comm.). Specifically we considered the three orthogonal axes of their Cartesian grid ($\hat{\mathbf{x}}, \hat{\mathbf{y}}, \hat{\mathbf{z}}$) in both positive and negative directions, resulting in six distinct radial profiles. The variation in spectral properties along the six directions compared to the spherically-averaged model partly reflects variations in abundance (Fig. 3). The remaining variation results from differences in the temperature and ionisation structures due to variations in the ^{56}Co distribution along the different directions, in particular above $\sim 4000\,\mathrm{km\,s^{-1}}$. The impact is most readily seen in the optical Fe III-dominated complex around $\sim 0.5\,\mu$m. By comparing Figs. 2 and 3 we see that the spectroscopic variation along different lines of sight in the DDT model can be as large as when considering different explosion models. This impacts the accuracy of abundance determinations when using spherically-averaged ejecta as well as our ability to make quantitative comparisons with observations.

4 Conclusions

We have compared four classes of public state-of-the-art SN Ia explosion models to nebular observations of SN 2021aefx covering the full 0.35–14 μm range. Our main result is that no single model emerges as an obvious candidate for SN 2021aefx based on these data alone. All models predict the same set of spectroscopic features, all of which have an observed counterpart. Conversely, all models lack specific characteristics of the observed

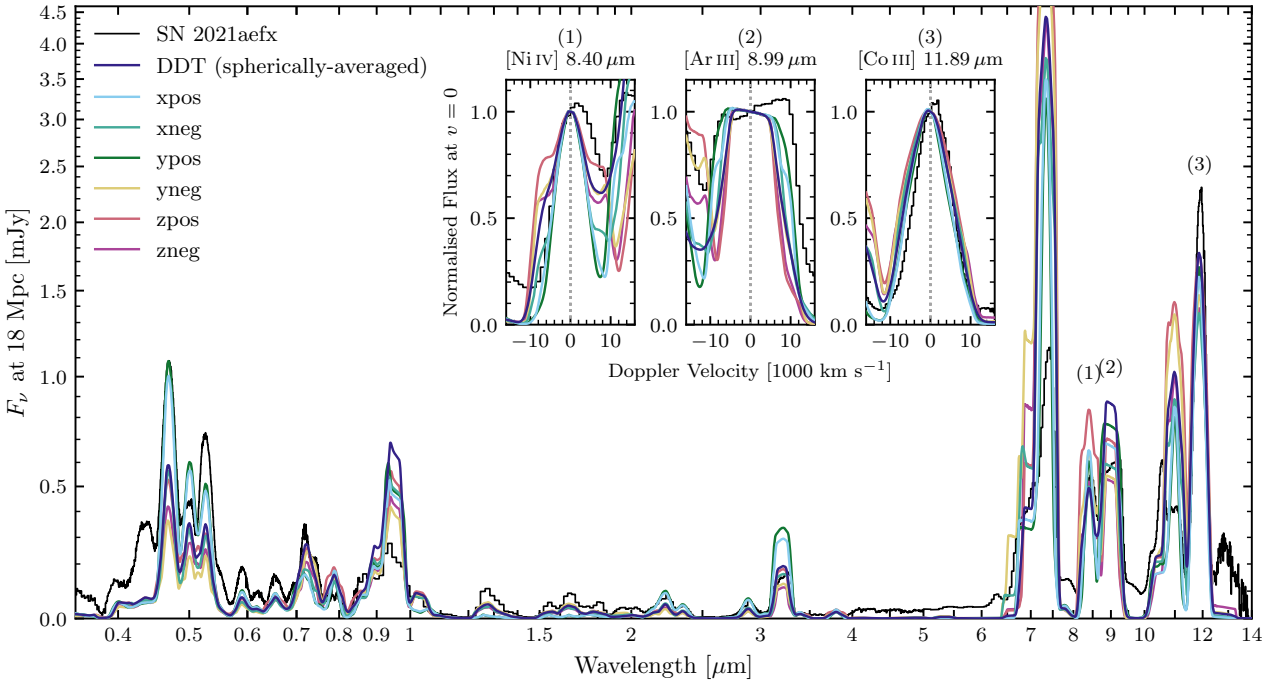

Fig. 3. Similar to Fig. 2 but for the DDT model along the three orthogonal axes of the original 3D Cartesian grid, in both positive ({x,y,z}pos) and negative ({x,y,z}neg) directions. We also show the original (spherically-averaged) DDT model.

spectrum, such as the overall mismatch in lines of singly-ionised IGEs throughout the optical and infrared. The largest variations in our model spectra result from differences in ionisation. A larger density, such as in the inner ejecta of the MERGER model, results in a lower ejecta temperature and ionisation state, further enhanced by the increased recombination rate.

In Blondin et al. (2023) we also discuss the use of lines of Ni I–IV in constraining the stable nickel mass, which could serve as a tracer of the mass of the exploding WD. Our investigation led to the computation of new collisional strengths for Ni III, available at the CDS.

Inferring reliable constraints on the progenitor mass and explosion mechanism of SNe Ia remains a formidable challenge, even with the extended wavelength coverage and exquisite data quality offered by *JWST*. Combined with early-time and optical observations, nebular infrared spectra of SNe Ia provide an additional validation criterion when comparing a diverse set of SN Ia models to observations.

This work was supported by the 'Programme National de Physique Stellaire' (PNPS) of CNRS/INSU co-funded by CEA and CNES. This research has made use of computing facilities operated by CeSAM data centre at LAM, Marseille, France.

References

Blondin, S., Bravo, E., Timmes, F. X., Dessart, L., & Hillier, D. J. 2022, A&A, 660, A96
Blondin, S., Dessart, L., Hillier, D. J., Ramsbottom, C. A., & Storey, P. J. 2023, arXiv e-prints, arXiv:2306.07116
Flörs, A., Spyromilio, J., Taubenberger, S., et al. 2020, MNRAS, 491, 2902
Gronow, S., Collins, C. E., Sim, S. A., & Röpke, F. K. 2021, A&A, 649, A155
Kromer, M., Ohlmann, S., & Röpke, F. K. 2017, Mem. Soc. Astron. Italiana, 88, 312
Kwok, L. A., Jha, S. W., Temim, T., et al. 2023a, ApJ, 944, L3
Kwok, L. A., Siebert, M. R., Johansson, J., et al. 2023b, arXiv e-prints, arXiv:2308.12450
Lach, F., Callan, F. P., Sim, S. A., & Röpke, F. K. 2022, A&A, 659, A27
Maoz, D., Mannucci, F., & Nelemans, G. 2014, ARA&A, 52, 107
Pakmor, R., Kromer, M., Taubenberger, S., et al. 2012, ApJ, 747, L10
Seitenzahl, I. R., Ciaraldi-Schoolmann, F., Röpke, F. K., et al. 2013, MNRAS, 429, 1156